IEEE Access
Multidisciplinary | Rapid Review | Open Access Journal

Received August 3, 2016, accepted August 31, 2016, date of publication September 19, 2016, date of current version October 6, 2016.

Digital Object Identifier 10.1109/ACCESS.2016.2610721

On Dimensions of OTA Setups for Massive MIMO Base Stations Radiated Testing

PEKKA KYÖSTI[1,2], WEI FAN[3], GERT FRØLUND PEDERSEN[3], AND MATTI LATVA-AHO[2]

[1]Keysight Technologies Finland Oy, 90590 Oulu, Finland
[2]Centre for Wireless Communications, University of Oulu, 90014 Oulu, Finland
[3]Department of Electronic Systems, Faculty of Engineering and Science, Antennas Propagation and Radio Networking Section, Aalborg University, 9100 Aalborg, Denmark

Corresponding author: P. Kyösti (pekka.kyosti@keysight.com)

This work was supported by the Innovation Fund Denmark via the Virtusuo Project. The work of W. Fan was supported by the Financial assistance from the Danish council for Independent Research under Grant DFF 6111-00525.

ABSTRACT The development of base stations (BSs) with large aperture antenna arrays, enabled partially by the utilization of cmWave and mmWave frequency bands, will require radiated testing in fading conditions. In this paper, the objective is to investigate the suitable measurement distances and physical dimensions of the over-the-air setups for the performance evaluation of massive multiple-input multiple-output (MIMO) BSs in anechoic chambers with multiple probes. Setup dimension is the major cost factor in the test systems and is thus the key issue to be investigated. The purpose is to determine whether the conventional far field criteria must be followed when determining the range of the setup or if they can be relieved. The impact of limited test setup dimension on various metrics, e.g., far field criteria, field performance within the test area, system link budget analysis, direction of arrival estimation algorithm as well as multi-user MIMO sum-rate capacity are investigated to determine the range of the test setup. It was found that the link budget does not support for the measurement distances claimed by the Fraunhofer distance. Most of the utilized metrics, especially the sum rate capacity, indicate that smaller setup sizes can still yield reasonable measurement accuracy. Simulations were performed at 2.6, 3.5, and 28 GHz frequencies.

INDEX TERMS Massive MIMO base station, performance evaluation, over the air testing, multi-probe anechoic chamber setup.

I. INTRODUCTION

Over-the-air (OTA) testing (also called radiated testing) of antenna system performance has the advantage, compared to conducted testing, of not needing to break or otherwise modifying the radio device. OTA testing for user equipment (UE) terminals with single antenna systems was standardized by The Wireless Association (CTIA) about ten years ago [1]. For single antenna UE systems, solely antenna gain-related parameters, i.e. total radiated power and total isotropic sensitivity, are specified for performance evaluation. The former is a measure of how much power is radiated by an antenna, while the latter is a measure of the average sensitivity of a receiver-antenna in an active system. OTA testing for UE terminals with multiple antenna systems has been under research, development and standardization for several years. Multi-probe anechoic chamber (MPAC) method is recently standardized in CTIA [2], while in 3GPP the work is still ongoing [3]. With the MPAC method, the radio propagation environment is reproduced as it would be experienced by the device under test (DUT) in the intended environment, but in a repeatable and controllable manner.

Massive multiple-input multiple-output (MIMO) systems, where radio base stations are equipped with a very large number of antennas, is seen as an enabling technology to fulfill dramatic improvements in spectral efficiency for 5G deployment in 2020 [4], [5]. OTA testing of such BS systems is essential due to several reasons. Conducted testing is undesirable due to the setup complexity associated with high number of cable connections. More importantly, radiated testing is indispensable, since according to an industrial view, future integrated BS units are foreseen not to support for any radio frequency (RF) cable connections for test purposes. This would prevent not only antenna related performance evaluations, but also any other fading tests that are traditionally performed conductively, like, e.g., standard 3GPP BS fading channel tests. Thus, there is a strong need to

develop suitable radiated testing methods for massive MIMO BS systems. MPAC systems are attractive for radiated testing of such systems, since the testing can be performed in a shielded environment, excluding unintended external interference. A BS designer has the possibility to quickly validate the BS performance in controllable radio environments in the early development stage. Various realistic propagation environments can be emulated as well in MPAC setups. It is worth of noticing that the geometry based channel models, such as WINNER [6], METIS [7], or the recent 3GPP channel model for above 6 GHz frequency [8], are naturally the most suitable for MPAC test setups as described in [9].

There are many concerns over the cost of the OTA testing of BSs equipped with massive antenna arrays. The cost of MPAC setups depends directly on its design. Key aspects include, e.g. the physical dimension of the setup (i.e. range between the probe antenna and the test device), number of required probe antennas (also respective number of required fading emulators), probe configuration, etc. The physical dimension of the setup is a key parameter in practical design of MPAC setups. While probe antennas, instrumentation and the anechoic chamber may be expensive, still in many cases the the floor space of the laboratory and the building around it may bring in the highest cost. Small MPAC setup is preferable, since it is more cost-effective and space-saving. However, unlike OTA testing for UEs where the diameter of a probe configuration is typically between 2.5 and three metres, the electrical size of the massive MIMO BS is much larger. Therefore a large test facility would be required, as demonstrated in the paper. On the other hand, a large test facility is more expensive, where extensive amplification units might be needed to meet the link budget requirement in large setups, which is not practical in reality.

In this paper, we intend to investigate the physical dimensions of MPAC setups that are suitable for radiated testing of massive MIMO BSs. Very limited work has been reported in the literature to address this aspect. For UE testing, the physical dimension of MPAC setups was investigated merely based on field performance over the test area and CTIA far field criteria below 6 GHz [10]. The MPAC setup for radiated testing of massive MIMO BSs has different requirements, as explained in section II. In this paper, a comprehensive analysis on the physical dimensions of MPAC setups for BSs is performed. The frequencies of particular interest in the paper are 2.6 GHz, 3.5 GHz and 28 GHz.

II. MPAC SETUPS FOR MASSIVE MIMO BSs

Commonly in cellular scenarios, the BS is placed higher and further away from scatterers (i.e. buildings, trees, cars, etc.). Therefore, it is expected that the angle profiles of the impinging power spectra at the BS side are more specular and confined in an angle region. For example the measurement based parametrization of WINNER UMi line-of-sight scenario [6] has rms angular spreads of 3° and 25° for the BS and UE sides, respectively. Sector antennas are used extensively at the BS side in the current systems. Typical angular coverage regions for a BS sector antenna are, e.g. 60°, 90° and 120° in azimuth domain. It is expected that BSs with massive antenna elements will cover a sectored angle region as well in the future deployment.

As for the UE side, since the scatterers are often nearby and located around the UE, the angle profiles would be less-specular (i.e. angle spread of the impinging power angle spectra might be large). Moreover, it is often assumed that channel models are confined to the azimuth domain and the elevation spread of the incoming power spectrum is concentrated on a very narrow elevation-angle region, since the BS is located far away. Furthermore, multipath channel can impinge the UE from arbitrary directions, i.e. not spatially confined in certain angle region.

Besides the differences in propagation environments seen by the BS and the UE, knowledge of the antenna characteristics might be different. For the UE, antenna locations are typically unknown, and the element radiation pattern is often quasi-omnidirectional with unknown polarization. As for the BS, the antenna locations are often known, and the antenna elements are often directive with known polarization characteristics.

To be able to reconstruct the typical real-world propagation environments at the UE side in the laboratory for radiated UE performance evaluation, a uniform 2D MPAC setup is often adopted, as shown in Figure 1 [2], [9]. This is due to the fact that multipath components impinging the UE from arbitrary directions in the azimuth plane are expected, as explained earlier. A 3D setup can be utilized for 3D spatial channel models as well [11]. Note that the target test area for 2D MPAC setup is often a circular geometry area on the azimuth plane.

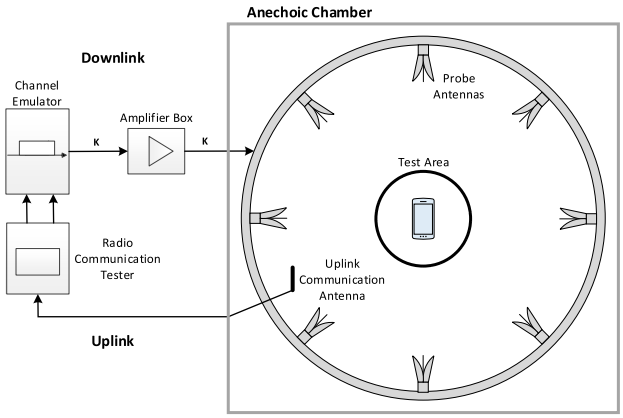

FIGURE 1. An illustration of the MPAC setup for UE performance evaluation.

An illustration of the proposed MPAC setup for BS performance evaluation is shown in Figure 2. To mimic the real-world propagation environment at the BS side and to save setup cost, a 3D sectored probe configuration is adopted. Furthermore, the BS should be evaluated as it is placed in the real-world, i.e. a test area in the elevation plane, as illustrated in Figure 3.

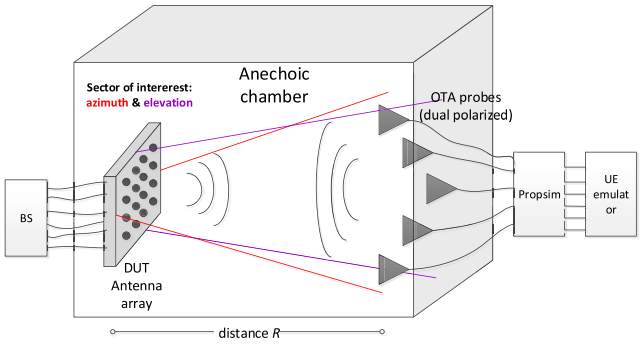

FIGURE 2. An illustration of the MPAC setup for massive MIMO BS performance evaluation.

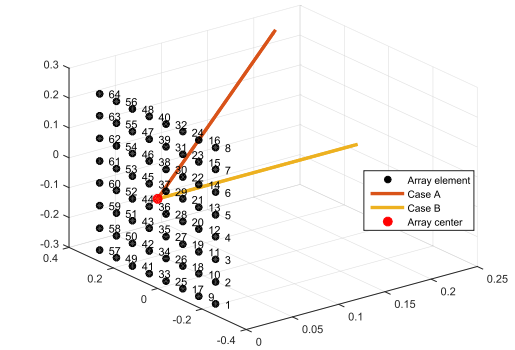

FIGURE 3. An illustration of the planar array. Case B denotes a probe from angle $\theta = 0°$ and $\phi = 0°$ and case A denotes a probe from angle $\theta = 30°$ and $\phi = 60°$.

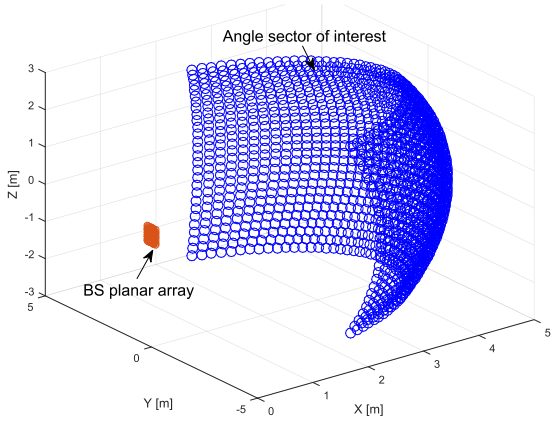

FIGURE 4. Chamber setups with R = 5 m.

In this paper, a uniform planar array of 8×8 antenna elements with 0.65λ element spacing is assumed for the BS. The test area is therefore a vertical square of size $4.55\lambda \times 4.55\lambda$ (e.g. 0.52 m $\times$0.52 m at 2.6 GHz), as shown in Figure 3. Furthermore, it is assumed that the BS DUT covers a 120° sector of azimuth angles and 60° sector of elevation angles centered at the broad side of the planar array. The sector of space angles is sampled by a sufficient number of probes at equal distance from the centre of the DUT, which is the origin of the coordinate system as illustrated in Figure 4. Thus the probes are located on a spherical surface. Note that the number and exact locations of the probes are exemplary only. In this paper, the elevation angle θ is measured from the xy plane to the z axis, and azimuth angle ϕ are measured counter-clockwise (top view) from the x axis on the xy plane. As a result, the planar array boresight direction is from angle $\theta = 0°$ and $\phi = 0°$, i.e. case B illustrated in Figure 4.

Different MIMO modes have different preferences for antenna array element spacing in the LTE base stations [12]. For transmit diversity and single-user spatial multiplexing purposes, large antenna element spacing is desired to achieve low antenna correlation. While for beamforming applications antenna element spacing is small at the BS side. BS array with small element spacing can reduce the BS size. However, the effect of mutual coupling may be more serious when the element spacing gets smaller. Array spacing below 0.5λ is rare in practical installation. The antenna spacing is selected to be 0.65λ in this paper. In [13] is shown by measurements an increase of multi-user MIMO performance when increasing the BS antenna element spacing even to a multitude of wavelengths. Interestingly, in their experiment the performance increase was saturated in many cases when the Fraunhofer distance reached the BS-UE distance.

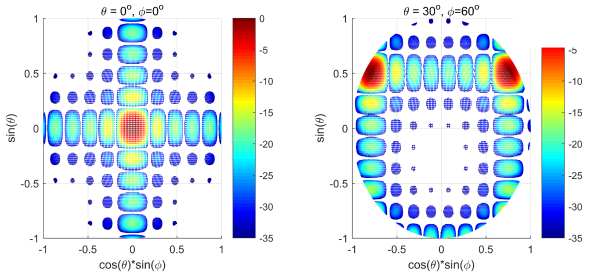

FIGURE 5. Three-dimensional antenna patterns of the planar array with isotropic elements with a element spacing 0.65λ with equal amplitude for $\theta = 0°$ and $\phi = 0°$ (left) and $\theta = 30°$ and $\phi = 60°$ (right).

The three-dimensional antenna patterns of the planar array with isotropic elements with equal amplitude is shown in Figure 5 for the angle in the centre of the sector (i.e., $\theta = 0°$ and $\phi = 0°$, as illustrated as case B in Figure 3) and the angle for one edge of the sector (i.e. $\theta = 30°$ and $\phi = 60°$, as illustrated as case A in Figure 3). As we can see in Figure 5 (left), a peak is formed at the boresight direction in the array pattern without any grating lobes, as expected [14]. However, for the angle from the edge of the sector, a grating lobe at $\theta = 30°$ and $\phi = -60°$ is formed in the pattern as well, as shown in Figure 5 (right). Note that grating lobes can be removed with antenna element spacing less than $\lambda/2$ [14].

III. LINK BUDGET ANALYSIS

If the physical dimension of the MPAC setup is large, we need to have extensive amplification units to ensure suitable signal strength levels for the BS DUT, and therefore link budget essentially limits the physical dimension of practical setups. In this section, the purpose is to evaluate how different

components of the setup would affect the overall power budget and to investigate how long distances R can be supported at different frequencies with hardware limitations in practical setups. Note that the link budget analysis at 2.6 GHz and 3.5 GHz in this section are based on current LTE parameter settings. It is expected that future 5G cellular systems at mm-Wave bands are widely different from current LTE systems. For example, the system bandwidth would be much wider. System settings and requirements for mm-Wave cellular systems are not clear at this stage. Therefore, link budget analysis at 28 GHz is left out here.

An illustration of main components of the test system for link budget analysis is shown in Figure 6. The parameter values for link budget calculation are detailed in Table 1, where different values at 3.5 GHz are marked in blue.

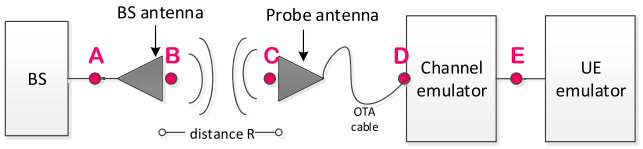

FIGURE 6. Definition of different points of the link budget calculation.

TABLE 1. Link budget analysis.

Input	Unit	$f_c =$ 2.6 GHz	$f_c =$ 3.5 GHz
Distance	[m]	5	3.5
Free space path loss	[dB]	54.7	54.3
BS Tx power $P_{TX,BS}$	[dBm]	43	43
BS antenna gain G_{TX}	[dBi]	5	5
Probe antenna gain G_P	[dBi]	6	6
Channel emulator gain G_{CE}	[dB]	-35	-35
UE transmit power $P_{TX,UE}$	[dBm]	23	23
OTA cable loss G_c	[dB]	3.1	3.5
Cable length	[m]	15	15
System bandwidth	[MHz]	20	20
Downlink	Unit	value	Point
BS Tx connector	[dBm]	43	A
BS antenna	[dBm]	48	B
Probe antenna	[dBm]	-6.7	C
channel emulator input connector	[dBm]	-3.8	D
channel emulator output connector	[dBm]	-38.8	E
UE input power [20 MHz]	[dBm]	-38.8	E
EPRE (power/15 kHz)	[dBm]	-70	E
Uplink	Unit	value	Point
UE Tx connector	[dBm]	23	E
Channel emulator input connector	[dBm]	23	E
channel emulator output connector	[dBm]	-12	D
Probe antenna	[dBm]	-9.1	C
BS antenna	[dBm]	-63.8	B
BS Rx connector [20 MHz]	[dBm]	-58.8	A
EPRE (power/15 kHz)	[dBm]	-90	A

For the downlink (i.e. from the BS to the UE emulator), the power value at the UE emulator input can be calculated in decibels as:

$$P_E = P_{TX,BS} + G_{TX} - 10\log 10\left[\left(\frac{4\pi \cdot R \cdot f_c}{c}\right)^2\right] + G_P - G_c + G_{CE}, \quad (1)$$

where the cable loss $G_c = 3.1$ dB and 3.5 dB are specified for $f_c = 2.6$ GHz and 3.5 GHz, respectively. The other parameter values are detailed in Table 1. Similarly, the power value at the BS input in the uplink in decibels (i.e. from the UE emulator to the BS) is:

$$P_A = P_{TX,UE} + G_{CE} - G_c + G_P - 10\log 10\left[\left(\frac{4\pi \cdot R \cdot f_c}{c}\right)^2\right] + G_{TX} \quad (2)$$

It is assumed that the BS transmit power is $P_{TX,BS} = 43$ dBm (around 20 watts) and the UE transmit power is $P_{TX,UE} = 23$ dBm (~0.2 watts). Based on experience gained on throughput measurement of LTE devices, the maximum performance (with 64 quadrature amplitude modulation (QAM) schemes and spatial multiplexing transmission modes) is achieved typically at lowest around −90 dBm Energy Per Resource Element (EPRE). Thus −90 dBm EPRE is taken as the target for the downlink. Note that the EPRE indicates power for each resource element (i.e. with one subcarrier bandwidth, e.g. 15 kHz for LTE systems). For a 20 MHz LTE system, the power value can be calculated in decibels as:

$$P_{20MHz} = EPRE_{15kHz} + 10 \cdot \log 10(20/0.015) \quad (3)$$

The power at BS connector is targeted at minimum −90 dBm EPRE as well for the uplink. Note that the uplink is more seriously power limited, since the UE transmit power is 20 dB lower in the uplink than the BS transmit power in the downlink. That is, it is more difficult to achieve −90 dBm EPRE at the BS Rx connector in the uplink and therefore the chamber dimension R is limited by the link budget in the uplink. As shown in Table 1, −70 dBm EPRE can be achieved for the downlink, while only −90 dBm EPRE is feasible for the uplink with the same R. For Table 1 the maximum distance R to achieve −90 dBm uplink Rx power was determined. It is 5 m at 2.6 GHz, and 3.5 m at 3.5 GHz, respectively. Larger R would require higher antenna gains or additional amplification. External power amplification would raise the calibration complexity substantially and it is preferably avoided. The free space loss and cable losses increase with higher frequencies, and therefore R would be reduced.

Note that the link budget analysis is only an approximation. For example, it is not known to the authors what the practical Rx power requirement of BS is. Also the channel emulator part, i.e. channel emulator gain G_{CE}, is dependent on the channel model and emulation settings. The values used in the analysis are based on typical settings of Keysight Propsim in UE OTA testing. Furthermore, the calculated link budget is from a single probe antenna to a single BS antenna. In practice, there are array gains at both end (between points A and D) that would impact the overall received power. The presented evaluation is a pessimistic calculation neglecting array gains. However, there may be channel models and cases where only very few probes are utilized for transmission/reception. E.g., if an UE is in strong LOS condition with AoD overlapping with a probe direction, then only that single probe would be utilized.

IV. METRICS FOR *R*

A. FAR FIELD CRITERIA

1) CTIA CRITERIA

CTIA test plan [1] specifies a minimum measurement distance R with three criteria, as below:

1) $R > 2D^2/\lambda$ (the Fraunhofer distance)
2) $R > 3D$
3) $R > 3\lambda$

These three criteria are applied to a BS DUT with the maximum dimension D of 6.4λ (i.e. the diagonal dimension of the BS DUT). Results of the three criteria are depicted in Figure 7. The size D scales with frequency, with $D = 0.74$ m and $D = 0.07$ m at 2.6 GHz and 28 GHz, respectively. The phase uncertainty criterion ($R > 2D^2/\lambda$) dominates the requirements at all frequencies. At low frequencies the DUT maximum diameter in metres is high and the minimum measurement distance R requirement is very demanding, with $R \geq 9.5$ m at 2.6 GHz. With the azimuth sector of 120°, the width of the chamber configuration would be 16.4 m, which would require floor area of well above 160 m^2. The physical dimensions required by the conventional CTIA far field criteria are much larger than those constrained by the link budget analysis in practical setups, as discussed in Section 1.

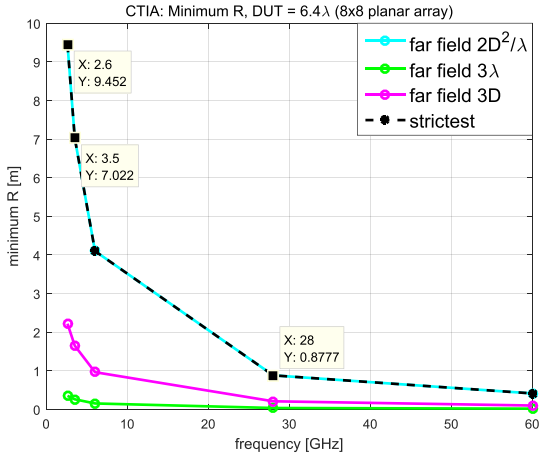

FIGURE 7. CTIA minimum measurement distance criteria with fixed DUT diameter D = 6.4λ as a function of frequency.

Conventional far field criteria are used to ensure that a plane wave is well approximated across the DUT aperture. These criteria are important for antenna parameter measurements, since far-field antenna pattern and antenna gain should be measured ideally under illumination of a uniform plane wave, which has a planar wave front with the field vectors being constant over an area that extends well beyond the aperture of the DUT. On the other hand, for performance evaluation of multiple antenna system in MPAC setups, the focus is to realistically evaluate link level and system level performance. At the moment, it is not clear whether conventional far field criteria should be met for this purpose. In the following sub-section, other metrics to evaluate dimensions of the test setup within an anechoic chamber are discussed to address this question.

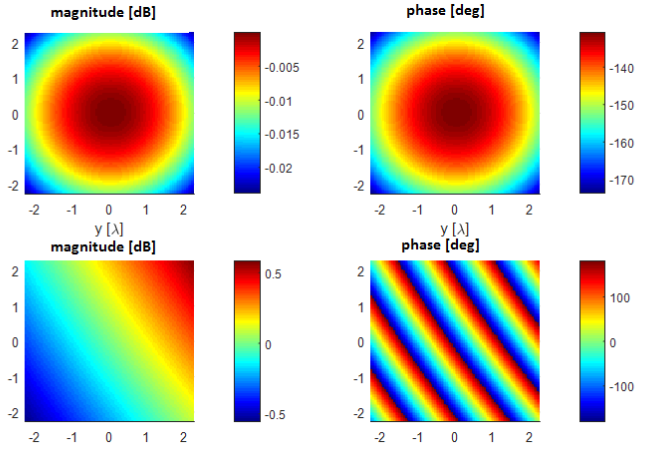

FIGURE 8. Magnitude and phase distribution over the test area for case A (top figures) and case B (below figures).

2) FIELD PERFORMANCE

Due to the large physical size for massive MIMO BS and limited R, magnitude distribution across the test area would vary and the phase front is curved. The field distributions over the test area for two representative probe antennas (i.e. case A and case B shown in Figure 3) are demonstrated in Figure 8 as examples. For the probe at $\theta = 0°$ and $\phi = 0°$, power variation less than 0.1 dB and phase deviation up to 43° are observed. As for the probe at $\theta = 30°$ and $\phi = 60°$, a power variation is up to 1.1 dB and phase front is slightly curved. $R = 5$ m and $f_c = 2.6$ GHz are set in the simulation in this subsection. In this part, statistics of the field distortions over the test area in terms of magnitude, angle and phase deviations are investigated.

a: MAGNITUDE DEVIATION

To obtain the statistics of magnitude distribution over the test area for all possible probe antenna locations within the sector of interest, we first calculate the path loss from a single probe location to all 64 DUT antenna locations and to the centre of DUT. Then the maximum deviation and the mean deviation are determined with respect to the DUT centre. The maximum and mean deviations are collected for all probe locations and the empirical cumulative distribution function is determined, as illustrated in Figure 9 for different frequencies. With the given setup, the mean magnitude deviation is always below 0.3 dB and the maxima are below 1.2 dB (as shown in case A in Figure 8). The deviation is largest at 2.6 GHz and lowest at 28 GHz.

b: ANGLE DEVIATION

Each probe location represents a certain space angle for the DUT. In ideal case, the space angle would be invariant as observed by different DUT antennas. However, the limited

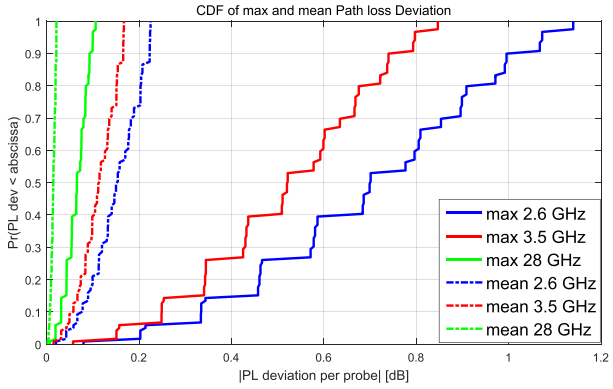

FIGURE 9. CDF of the max and mean magnitude deviation over the test area for $f_c = 2.6$ GHz, 3.5 GHz and 28 GHz.

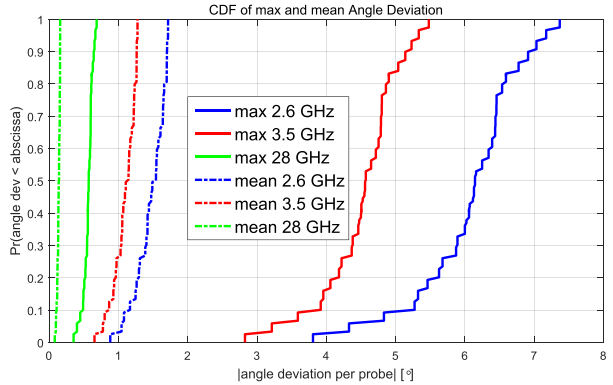

FIGURE 10. CDF of the max and mean angle deviation over the test area for $f_c = 2.6$ GHz, 3.5 GHz and 28 GHz.

distance R effectively causes variation in the space angle of a particular probe as observed by different locations on the test area. The angle deviation can be calculated as follows. The first vector is a segment of line from the test area centre to a probe antenna location. The second vector is the normal vector of the planar test area. The angle between the two vectors is calculated. Replacing the test area centre by each DUT antenna location, the angles can be calculated for all DUT antenna elements corresponding to the probe. Again, similar to the magnitude deviation, the maximum and mean angle deviation statistics are collected for the probe location. The process is repeated for all probe antennas and the CDFs are plotted in Figure 10. As we can see, the mean angle deviation is below 2° and the maximum deviation is less than 7.5° in all cases.

c: PHASE DEVIATION

The third metric is the phase deviation. Phase deviation is the phase difference between assumed plane wave from a probe location to the centre of the test area and the corresponding spherical wave determined by the distance R, as illustrated in Figure 11. In the test area centre, the plane and spherical wavefronts are synchronized, but off from the origin, there would be delay offset (phase difference) between the

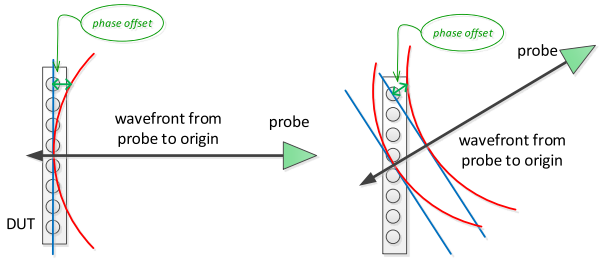

FIGURE 11. An illustration of the phase error across the DUT. Left illustrates the CTIA definition and right is the general definition.

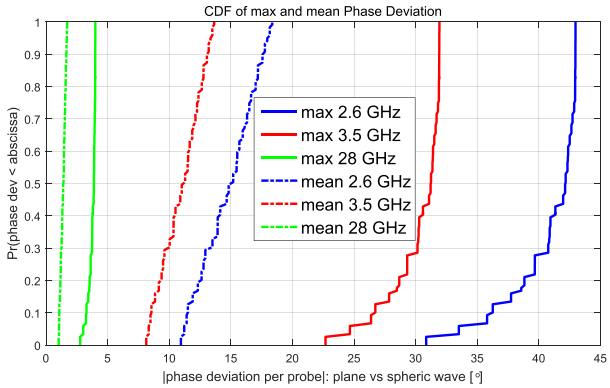

FIGURE 12. CDF of the max and mean angle deviation over the test area for $f_c = 2.6$ GHz, 3.5 GHz and 28 GHz.

wavefronts. The largest phase difference between the spherical wave and the plane wave appears at the edges of the BS DUT. In CTIA conventional far field criteria, the probe antenna is fixed in the boresight direction to calculate the phase deviation. In this paper, the phase deviation calculation is generalized to arbitrary arrival angles. As shown in Figure 11, if the probe was from array endfire direction (top view), the phase deviation would be zero on all DUT antenna locations. The phase deviation is calculated from all probes to all DUT antennas and similarly to the previous deviation metrics the statistics are collected. CDF curves are plotted in Figure 12. At 2.6 GHz, the mean phase deviation is between 10° and 18°, and the maximum deviation is between 30° and 43°. The highest phase error occurs from probes in the broad side direction of the DUT, as shown in Figure 8.

An obvious trend can be read from the deviation results: the requirement for R decreases with increasing measurement frequency. As explained earlier, it would be desirable to link the field deviations to any link level or system level performance metrics. It is for future work to find acceptance thresholds for the field deviations.

B. DIRECTION OF ARRIVAL (DoA) ALGORITHM PERFORMANCE

DoA estimation using antenna arrays has long been of research interest, where plane wave impinging is often assumed for DoA estimations [15]. In this section, we intend to investigate the impact of limited MPAC physical dimension

on two well-known DoA algorithms, namely the classical beamforming and MUSIC algorithms [15].

The received signal vector at time snapshot t can be written in matrix form as follows:

$$\boldsymbol{x}[t] = \mathbf{T}\boldsymbol{s}[t] + \boldsymbol{v}[t], \tag{4}$$

where

- $\boldsymbol{x}[t] \in \mathbb{C}^{M\times 1}$ is a vector containing M received signal samples at the t-th time snapshot. $M = 64$ denotes the number of BS antenna elements.
- $\mathbf{T} \in \mathbb{C}^{\mathrm{M}\times\mathrm{N}}$ is the static, R dependent, transfer matrix of coefficients from the $n-$th probe to the $m-$th antenna element. N is the total number of probes.
- $\boldsymbol{s}[t] \in \mathbb{C}^{N\times 1}$ is a vector containing N transmitted signal samples at the $t-$th time snapshot.
- $\boldsymbol{v}[t] \in \mathbb{C}^{M\times 1}$ is the noise vector. The noise term is neglected in this study.

In this paper, as the focus to investigate the impact of R on DoA estimation algorithms, narrowband and i.i.d Rayleigh distributed signal radiated from one probe (i.e. $N = 1$) is assumed for the sake of simplicity. In the simulation, two representative cases are selected:

1) one probe active at the boresight direction of the BS array (i.e. case B shown in Figure 3) with different Rs.
2) one probe active at the edge of the sector (i.e. case A shown in Figure 3) with different Rs.

Three different ranges $R = 5$m, 9.5m and ∞ are selected for each case. Note that $R = 9.5$m is the minimum CTIA far field distance at 2.6 GHz. The simulation frequency is set to be 2.6 GHz. The distance $R = 1000m$ is set to approximate $R = \infty$ in the simulation and used the reference case where all waves fronts are (almost) perfectly planar and no near field effects are present.

a: BEAMFORMING

Beamforming algorithm computes the angle by measuring the signal power at each possible angle of arrival and selecting the direction of maximum power as the estimate of the angle of arrival. The power angular spectrum is given by [15]:

$$\mathrm{P}_{\mathrm{beamformer}}(\theta,\phi) = \alpha^{H}(\theta,\phi)\hat{\mathbf{R}}\alpha(\theta,\phi), \tag{5}$$

where $\alpha(\theta,\phi) \in \mathbb{C}^{M\times 1}$ is the steering vector for the BS planar array. $\hat{\mathbf{R}} \in \mathbb{C}^{M\times M}$ is the auto-covariance matrix of the received signals.

b: MUSIC ALGORITHM

The MUSIC algorithm is utilized here as an example for the high resolution algorithm class. The MUSIC algorithm searches through the set of all possible steering vectors and find those that are orthogonal to the noise subspace [15]. The power angular spectrum is given by:

$$\mathrm{P}_{\mathrm{MUSIC}}(\theta,\phi) = \frac{1}{\alpha^{H}(\theta,\phi)\hat{\mathbf{G}}\hat{\mathbf{G}}^{\mathrm{H}}\alpha(\theta,\phi)}, \tag{6}$$

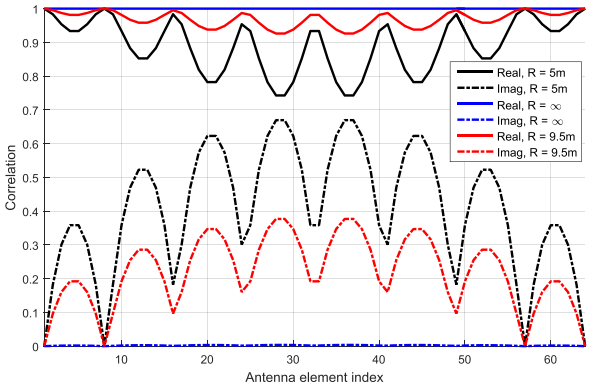

FIGURE 13. Real and imaginary component of the correlation coefficients of the received signals for case A.

where $\hat{\mathbf{G}} \in \mathbb{C}^{M\times M}$ is the noise subspace eigenvectors, which can be obtained from $\hat{\mathbf{R}}$ [15].

The real and imaginary components of the correlation coefficients between the received signals at antenna element 1 and the rest 63 elements are shown in Figure 13 for case A with different distances R. We can observe that the correlation of the received signals depends on R.

The results are shown in Figure 14 and Figure 15 for the classical beamforming and MUSIC algorithms, respectively. For case A, the target space angles can be correctly estimated with both DoA estimation algorithms. The beamforming algorithm, though suffering from high side-lobes and wide main beamwidth, is quite robust to imperfections introduced by the spherical wave front, with similar results achieved for $R = 5$m, 9.5 m and ∞. The MUSIC algorithm is superior in ideal plane wave case (i.e. $R = \infty$), offering low side lobes and narrow main beam-width. However, its performance is quite sensitive to errors introduced by spherical wave fronts, where a peak at target angle is only around 10 dB and 15 dB above the estimated values at other angles for $R = 5$m and $R = 9.5$ m, respectively.

For case B, the results will suffer from grating lobes as expected, since the antenna spacing is larger than 0.5λ. As shown in Figure 14 and Figure 15, besides the target space angle at $\theta = 30°$ and $\phi = 60°$, a peak is formed at $\theta = 30°$ and $\phi = -60°$ as well. Note that the grating lobe is caused by the large antenna element spacing in the BS array and therefore it exists for any chamber dimension.

C. MU-MIMO SUM RATE CAPACITY

Massive MIMO arrays at BSs can be utilized for multi-user MIMO (MU-MIMO) communications. BS is serving a number of UEs distributed in space simultaneously at the same frequency. In this sub-section we consider MU-MIMO sum rate capacity [16] as a metric to evaluate the impact of limited R. The distance $R = 1000$m is taken as the reference case where all waves fronts are (almost) perfectly planar and no near field effects are present.

We generated geometric propagation parameters and fading sequences at 2.6 GHz centre frequency for a single BS site

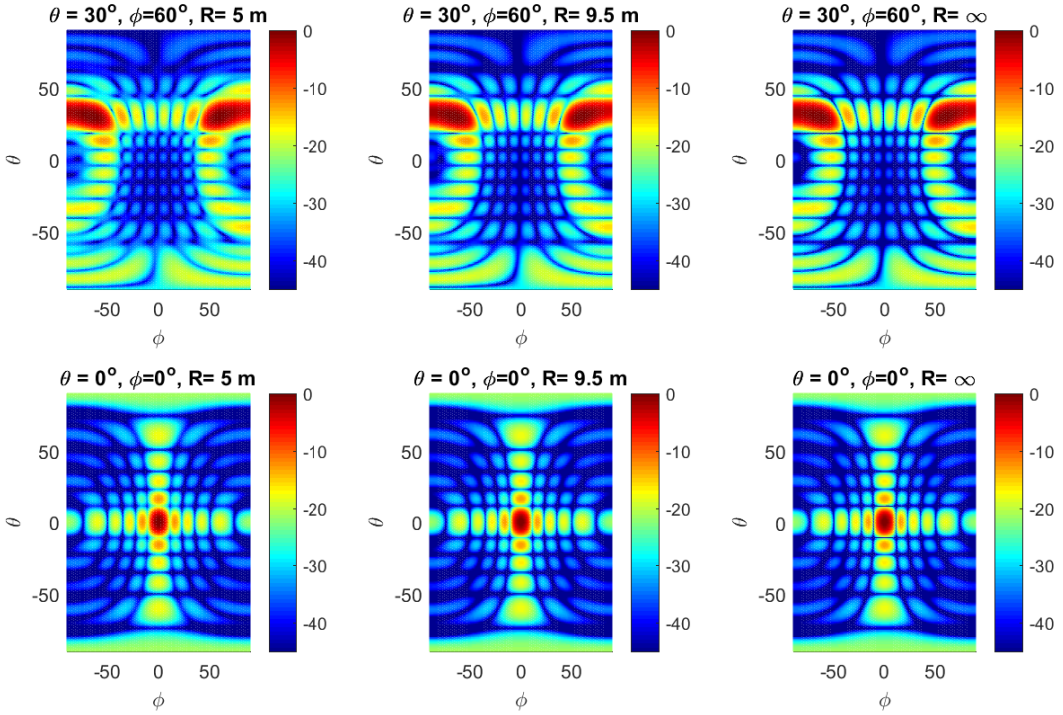

FIGURE 14. Simulated power angular spectra using the beamforming method for case A (bottom figures) and case B (top figures) with different R.

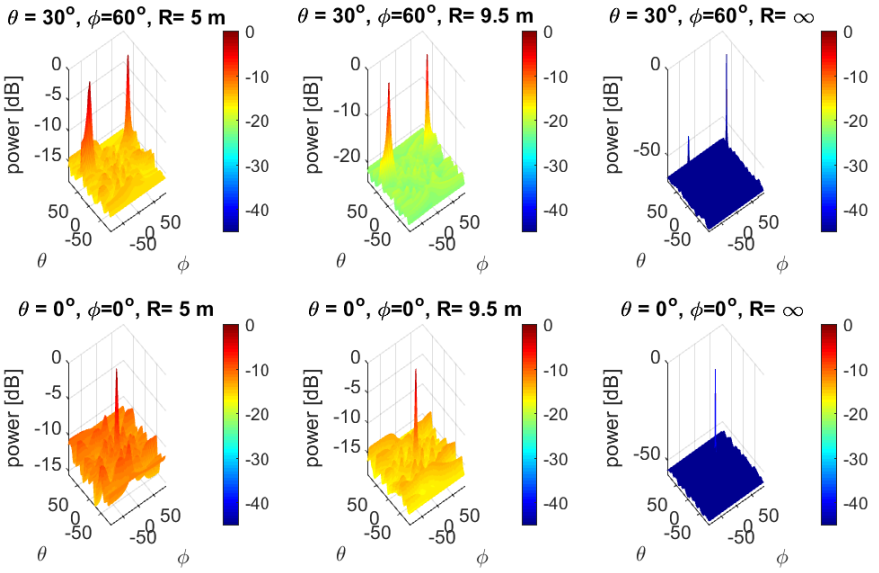

FIGURE 15. Simulated power angular spectra using the MUSIC method for case A (bottom figures) and case B (top figures) with different R.

and 30 single antenna UEs distributed randomly in a sector of 120 degrees with Anite Geometric Channel Modelling Tool. The channel model, i.e. the procedure to draw random parameters and channel realizations $\mathbf{H}^{\mathrm{GSCM}}(t)$, follow IMT-Advanced UMi scenario [17]. The nominal azimuth and elevation angles at BS side (AoD and EoD) of each multi-path l of each UE k were mapped to an example configuration of $N = 120$ probes, by allocating each path (k, l) a probe index $b_{k,l} \in [1, N]$, as illustrated in Fig 16. Thus the fading sequence of a path was radiated by a single probe. If there were paths with AoD or EoD outside the BS sector they were still mapped to the closest probes on edges of the probe geometry. BS antenna was the 8×8 planar array described earlier. Sub-sets of $K = 6$ UEs were picked randomly from

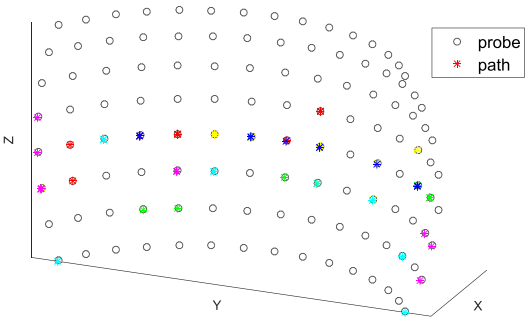

FIGURE 16. The probe configuration of MU-MIMO simulation and an example path allocation to probes. Each path is denoted by *, UEs are differentiated by colours.

the full set of 30 UEs. The 64 × 6 channel matrix $\mathbf{H}(t)$ was constructed by taking the fading sequences mapped to probes

$$F_{n,k}(t) = \sum_{l} H_{k,l}^{\mathrm{GSCM}}(t)\delta(n - b_{k,l}) \tag{7}$$

composing a matrix $\mathbf{F}(t) \in \mathbb{C}^{120\times 6}$ and utilizing the known static, distance R dependent, transfer matrix $\mathbf{T} \in \mathbb{C}^{64\times 120}$ from all probes to all BS antennas as

$$\mathbf{H}(t) = \mathbf{T}\mathbf{F}(t). \tag{8}$$

The channel matrix is normalized to have equal channel gain between UEs and overall unit gain over time samples.

As the next step linear pre-coding vectors were determined for each UE of the sub-set by the zero forcing method [16], which is a sub-optimal linear pre-coding and aims to achieve zero interference between users. The matrix composed of pre-coding vectors was calculated with the well known Moore-Penrose pseudo-inverse as follows

$$\mathbf{W}(t) = \mathbf{H}^H(t)\left(\mathbf{H}(t)\mathbf{H}^H(t)\right)^{-1} \tag{9}$$

after which the rows $\mathbf{w}_k(t)$ of $\mathbf{W}(t)$ were normalized. The sum rate capacity was calculated as [16]

$$C(t) = \sum_{k=1}^{K} \log_2\left(1 + \frac{\gamma}{K}\left|\mathbf{w}_k(t)\mathbf{h}_k(t)\right|^2\right), \tag{10}$$

where the signal-to-noise ratio $\gamma = 20$ dB and $\mathbf{h}_k(t)$ are column vectors of $\mathbf{H}(t)$.

The simulation was repeated for 500 random UE sub-sets each with 10000 time samples and for five different distance, namely $R = 1, 2, 5, 9.5, 1000$ metres, where the last 1000 m case represents the ideal condition of $R = \infty$. An empirical cumulative distribution function (CDF) of the sum rate capacity for a single sub-set is shown in Fig. 17. There the curve for distance $R = 1$m is clearly deviating and $R = 2$m is only slightly deviating from the reference curve of $R = 1000$m while the other curves are mostly overlapping. Finally, statistics of the sum rate capacity were calculated for the 500 random sub-sets. The result is depicted in

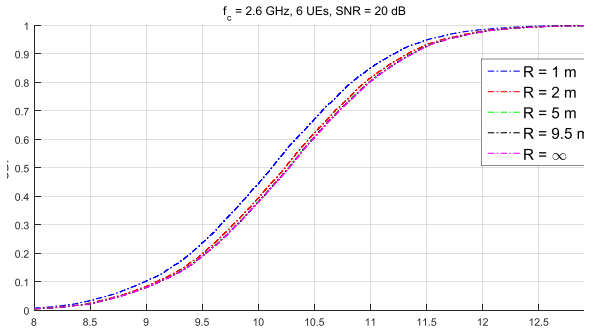

FIGURE 17. CDF of sum rate capacity for an example sub-set of six UEs.

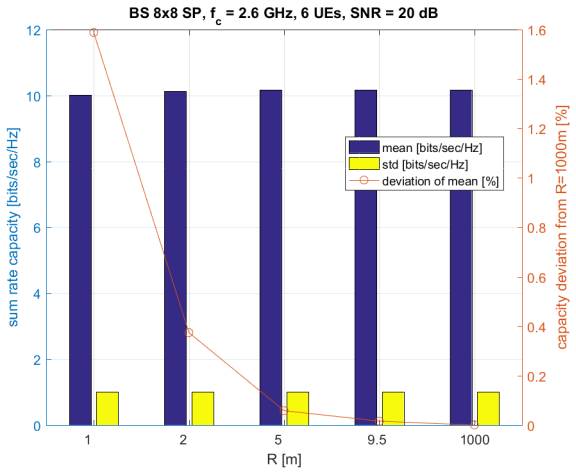

FIGURE 18. MU-MIMO sum rate capacities: mean, standard deviation and deviation from the $R = 1000$ m ($R = \infty$) case.

fig. 18, showing the mean of time averaged capacities over the 500 sub-sets and the average of standard deviations of instantaneous capacities over the 500 sub-sets. In addition fig. 18 contains the relative deviation of mean capacities from the reference, i.e. $R = 1000$m, capacity. Overall, the impact of the distance R is small, but the trend is clear. The deviation decreases when R increases towards the ideal case with perfect plane waves. It is hard to define any numerical threshold, but by comparing the deviation metrics and observing the example CDF curves, one could conclude that the MU-MIMO sum rate capacity converges with $R > 2$m.

V. CONCLUSION

We have introduced an MPAC setup for radiated testing of massive MIMO BSs, where probes are located in a confined space angle, i.e. a sector of azimuth and elevation directions, with a constant distance R from the test area centre. We assumed 120° and 60° azimuth and elevation sectors, respectively. Given this, the physical dimensions of the configuration are solely determined by R. In this paper we assessed the requirements for and implications of selecting certain values for R at specific frequencies. As an obvious general observation, increasing the measurement frequency

decreases the distance requirement for a BS with fixed electrical size.

Link budget calculations were done with approximated values from existing UE OTA tests and with the objective to avoid extensive power amplification units. The link budget indicates that the maximum distances R are 5 m and 3.5 m at 2.6 GHz and 3.5 GHz measurement frequencies, respectively.

Different metrics concerning performance of the generated fields were introduced and evaluated. With $R = 5$ m at 2.6 GHz the values of magnitude, angle, and phase mean deviations were below 0.3 dB, 2°, and 18°, respectively. The metrics lack exact acceptance criteria, nonetheless at least with the first two metrics the mean deviations can be considered small.

The impact of limited R on DoA estimation accuracy was assessed utilizing both the classical beamformer and MUSIC algorithms. The former was found robust, giving similar accuracy with $R = 5$, 9.5, and 1000 m distances. However, the latter is very sensitive to the curvature of impinging waves and the estimation noise level increased clearly when going from $R = 1000$ to $R = 9.5$ or $R = 5$ m. Thus even the Fraunhofer distance did't preserve from increased estimation noise.

As the last metric the MU-MIMO sum rate capacities were simulated. There the impact of R at 2.6 GHz was small, resulting to 1.6%, 0.4%, and below 0.1% deviations from the ideal case with $R = 1$, $R = 2$, and $R \geq 5$ m, respectively. This observation is in contrast to the traditional far field criteria. However, this is quite expected, while the latter is utilized for antenna measurements and with ideal plane waves, the former contains multi-dimensional fading channel with a multitude of radiating sources composing complex directional field structures. As a summary we tend to conclude that the Fraunhofer distance is not a precondition for R. With fading testing of massive BSs the measurement distance requirement can be relieved.

ACKNOWLEDGMENT

The authors would like to thank the help and discussions from Mrs. Fengchun Zhang with Aalborg University.

REFERENCES

[1] "Test plan for wireless device overthe-air performance: Method of measurement for radiated RF power and receiver performance," CTIA Certification, Tech. Rep. Version 3.5.2, Sep. 2015.
[2] "Test plan for 2x2 Downlink MIMO and transmit diversity over-the-air performance," CTIA Certification, Tech. Rep. Version 1.0, Aug. 2015.
[3] "Radiated performance requirements for the verification of multi-antenna reception of UEs," 3GPP RP-160603, Tech. Rep., Mar. 2016.
[4] E. G. Larsson, O. Edfors, F. Tufvesson, and T. Marzetta, "Massive mimo for next generation wireless systems," *IEEE Commun. Mag.*, vol. 52, no. 2, pp. 186–195, Feb. 2014.
[5] T. L. Marzetta, "Massive MIMO: An introduction," *Bell Labs Tech. J.*, vol. 20, pp. 11–22, Mar. 2015.
[6] P. Kyösti *et al.*, "WINNER II Channel Models, Deliverable 1.1.2 v.1.2," IST-4-027756 WINNER II, Tech. Rep., Sep. 2007. [Online]. Available: http://projects.celtic-initiative.org/winner+/deliverables.html
[7] L. Rachowski, P. Kyösti, K. Kusume, and T. Jämsä, Eds., "METIS channel models, Deliverable 1.4 v.1.3," METIS Project, Tech. Rep. ICT-317669, 2015.
[8] "Channel model for frequency spectrum above 6 GHz," 3GPP TR 38.900, Tech. Rep. Rel 14, V2.0.0, Jun. 2016.
[9] P. Kyösti, T. Jämsä, and J.-P. Nuutinen, "Channel modelling for multi-probe over-the-air MIMO testing," *Int. J. Antennas Propagat.*, vol. 2012, 2012, Art. no. 615954, doi:10.1155/2012/615954
[10] P. Kyösti and L. Hentilä "Criteria for physical dimensions of MIMO OTA multi-probe test setup," in *Proc. 6th Eur. Conf. Antennas Propag. (EUCAP)*, Mar. 2012, pp. 2055–2059.
[11] C. Schirmer *et al.*, "3D wave-field synthesis for testing of radio devices," in *Proc. 8th European Conference on Antennas and Propagation (EuCAP 2014)*, The Hague, 2014, pp. 3394–3398.
[12] R. Bhagavatula, R. W. Heath, Jr. and K. Linehan, "Performance evaluation of mimo base station antenna designs," *Antenna Syst. Technol. Mag.*, vol. 11, no. 6, pp. 14–17, 2008.
[13] G. Dahman, J. Flordelis, and F. Tufvesson, "Experimental evaluation of the effect of BS antenna inter-element spacing on MU-MIMO separation," in *Proc. IEEE Int. Conf. Commun. (ICC)*, Jun. 2015, pp. 1685–1690.
[14] C. A. Balanis, *Antenna Theory: Analysis and Design*. Hoboken, NJ, USA: Wiley, 2016.
[15] P. Stoica and R. L. Moses, *Spectral Analysis of Signals*. Upper Saddle River, NJ, USA: Prentice-Hall, 2005.
[16] F. Kaltenberger, D. Gesbert, R. Knopp, and M. Kountouris, "Correlation and capacity of measured multi-user MIMO channels," in *Proc. IEEE 19th Int. Symp. Pers., Indoor Mobile Radio Commun. (PIMRC)*, Sep. 2008, pp. 1–5.
[17] "Guidelines for evaluation of radio interface technologies for IMT-advanced," ITU-R, Tech. Rep. ITU-R M.2135-1, Dec. 2009.

PEKKA KYÖSTI received the M.Sc. degree in mathematics from the University of Oulu, Finland. From 1998 to 2002, he was with Nokia Networks. From 2002 to 2016, he was with Elektrobit/Anite. Since 2002, he has been involved in radio channel measurements, estimation and modeling. From 2008 to 2012, he was actively developing methods for MIMO over-the-air testing. He was moved to Keysight Technologies Finland Oy along the acquisition in 2016. He is currently involved in channel modeling for 5G systems with Keysight Technologies Finland Oy and with the University of Oulu.

WEI FAN received the B.E. degree from the Harbin Institute of Technology, China, in 2009, the master's degrees (Hons.) from the Politecnico di Torino, Italy, and the Grenoble Institute of Technology, France, in 2011, and the Ph.D. degree from Aalborg University, Denmark, in 2014. In 2011, he was with Intel Mobile Communications, Denmark, as a Research Intern. He conducted a internship with Anite telecoms oy, Finland, in 2014. His main areas of research are over the air testing of MIMO terminals, radio channel modeling, and virtual drive testing.

GERT FRØLUND PEDERSEN was born in 1965. He received the B.Sc. degree (Hons.) in electrical engineering from the Dublin Institute of Technology, Dublin, Ireland, in 1991, and the M.Sc. degree in electrical engineering and the Ph.D. degree from Aalborg University in 1993 and 2003, respectively. He has been with Aalborg University since 1993, where he is currently a Full Professor, where he is also heading the Antenna, Propagation and Networking Lab with 36 Researcher. He was also a Consultant for developments of over 100 antennas for mobile terminals including the first internal antenna for mobile phones in 1994 with lowest SAR, first internal triple-band antenna in 1998 with low SAR and high TRP and TIS, and lately various multi antenna systems rated as the most efficient on the market. He has been with joint university and industry projects. He is currently the Project Leader of the SAFE Project with a total budget of 8 M$ investigating tunable front end including tunable antennas for the future multiband mobile phones. He has been one of the pioneers in establishing over-the-air (OTA) measurement systems. The measurement technique is now well established for mobile terminals with single antennas. He is also the Head of the Doctoral School on wireless communication with some 100 Ph.D. students enrolled. He has authored over 175 peer-reviewed papers and holds 28 patents. His research has focused on radio communication for mobile terminals especially small antennas, diversity systems, propagation, and biological effects. He was the Chair of the various COST groups (swg2.2 of COST 259, 273, 2100, and now ICT1004) with liaison to 3GPP for OTA test of MIMO terminals and he is currently deeply involved with MIMO OTA measurement. He have received over 12 M$ in direct research funding.

MATTI LATVA-AHO received the M.Sc., Lic.Tech., and Ph.D. (Hons.) degrees from the University of Oulu, Finland, in 1992, 1996, and 1998, respectively, all in electrical engineering. From 1992 to 1993, he was a Research Engineer with Nokia Mobile Phones, Oulu, Finland. He joined the Center for Wireless Communications (CWC), University of Oulu. He was the Director of the CWC from 1998 to 2006, and the Head of Department for Communication Engineering until 2014. He is currently a Professor of Digital Transmission Techniques with the University of Oulu. He has authored over 300 conference or journal papers in wireless communications. His research interests are related to mobile broadband communication systems and currently his group focuses on 5G systems research. He received the Nokia Foundation Award in 2015 for his achievements in mobile communications research.